The III-Nitrides as a Universal Compound Semiconductor Material: A Review

Chuanle Zhou[a], Amirhossein Ghods[a], Vishal G. Saravade[a],
Paresh V.Patel[a], Kelcy L. Yunghans[a], Cameron Ferguson[a], Yining Feng[b],
Xiaodong Jiang[b], Bahadir Kucukgok[b], Na Lu[b], and Ian T. Ferguson[a]

[a] Electrical and Computer Engineering,
Missouri University of Science and Technology, Rolla MO 65409
[b] Lyles School of Civil Engineering, School of Materials Engineering,
Birck Nanotechnology Center, Purdue University, West Lafayette, IN 47907, USA

III-nitrides are attracting considerable attention as promising materials for a wide variety of applications due to their wide coverage of direct bandgap range, high electron mobility, high thermal stability and many other exceptional properties. The light-emitting diodes based on III-nitrides revolutionize the solid-state lighting industry. III-nitrides based solar cells and thermoelectric generators support the sustainable energy progress, and the III-nitrides are better alternatives for power and radio frequency (RF) electronics compared with silicon. The doped III-nitrides' magnetic properties and sensitivity to radiation can contribute to novel spintronic and nuclear detection devices. This paper will review III-nitride material properties and their corresponding applications in LEDs, solar cells, power and radio frequency (RF) electronics, magnetic devices, thermoelectrics and nuclear detection. The typical values of electrical, optical, thermoelectric, magnetic properties are cited, the current state of art investigations are reported, and the future applications are estimated.

Introduction

The III-nitrides, typically composed of GaN and its alloys with Al and In, are compound semiconductor materials with superior properties and well developed growth techniques (1) that assure extensive progress in various applications. The III-nitrides have a hexagonal wurtzite structure and a continuous alloy system with tunable direct bandgaps from 6.2 eV (AlN) across 3.4 eV (GaN) to 0.7 eV (InN) (2) (Figure 1). This wide coverage of direct bandgap range from deep-ultraviolet (UV) to infrared region promises a variety application in optoelectronics, such as light-emitting diodes (LEDs), lasers, photodetectors and solar cells. GaN is recognized with high breakdown field, high thermal conductivity, and high electron mobility, making GaN an excellent candidate for high power and RF electronic devices. III-nitrides exhibit high Seebeck coefficient and excellent temperature stability for high temperature thermoelectric applications. Doped GaN shows other special properties and applications, such as transition/rare-earth metals doped GaN with magnetic properties, and indium (In)/gadolinium (Gd)/boron (B)/and lithium (Li) doped GaN for nuclear detection.

This paper will review various applications of III-nitrides in the sequence of LEDs, solar cells, power and RF electronics, magnetic properties, thermoelectrics and nuclear detection applications, with their development history, current state of art and future explorations.
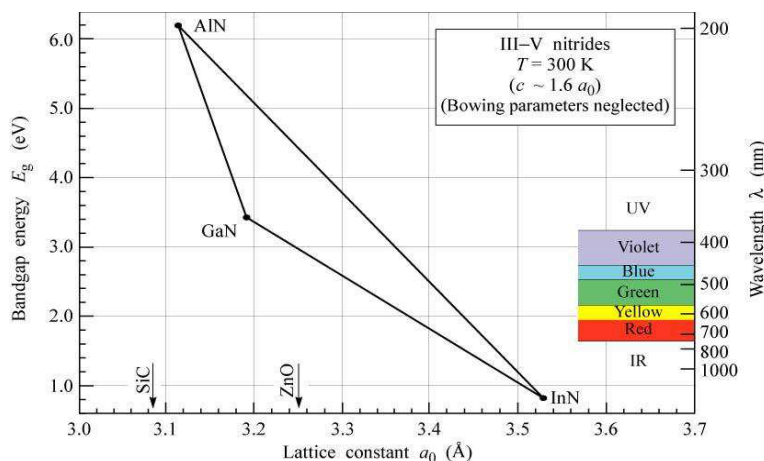

Figure 1 Bandgap vs. lattice constant for III-nitrides (2)

The III-Nitrides for Light-Emitting Diodes

Light-Emitting Diodes are a type of solid state lighting (SSL) with compact size, high energy efficiency and long lifetime. High brightness LEDs have various application in traffic lights, automobile brake lights and panel lights, indicator lights, mobile keyboards and displays, flat panel displays, and general lightings. III-nitrides (Ga, In, Al-N)-based LEDs play revolutionary role in the SSL market due to their wide emission spectrum covering UV, violet, blue and green, high efficiencies, and abilities for mass production (1-3).

The first GaN-based LEDs were fabricated using MIS structure (4) in RCA in 1971, with an output power of 1-5 μW. As the development of AlN or GaN buffer layers by molecular beam epitaxy (MBE) (5) and metalorganic chemical vapor deposition (MOCVD) (6,7), the quality of GaN film grown on sapphire substrate improved greatly. P-type GaN was achieved by Amano et al. in 1989 (8), and the hole compensation mechanism was clarified in 1992 (9). The first p-n junction GaN LED was reported by Nakamura et al. in 1991 with an output power and external quantum efficiency (EQE) of 42 μW and 0.18%, respectively (10). GaN has a direct bandgap of 3.45eV, corresponding to near UV light. Therefore, mixed alloys of (Al, In, Ga)N for band engineering is a hallmark for UV and visible light LEDs. High-quality InGaN layer on GaN on sapphire substrate demonstrated the first p-GaN/n-InGaN/n-GaN double-heterostructure (DH) blue LED in 1993 (11). Commercially available blue and green LEDs using InGaN quantum-well (QW) structures were demonstrated in the mid-1990s, and the output power and EQE of these LEDs were in the order of 3-5 mV and 6-9%, respectively (12,13,14). Time-resolved photoluminescence (TRPL) can be used to examine topological disorder from In phase segregation in wafers and prescreen InGaN LEDs before the final stages of processing (15).

LED light extraction efficiency was a major challenge for the III-nitrides LEDs. A considerable fraction of light was trapped within the LEDs by total internal reflection (TIR), due to the large differences in the reflection indices of GaN (n~2.4) and sapphire substrate (n~1.8). Patterned sapphire substrates (PSSs) (16) or roughening in vertical LEDs (VLEDs) achieve light extraction efficiencies of over 80% today (17,18). Methods are still under investigation to reduce TIR by surface roughening (19), substrate patterning, chip shape optimization, and material integrating/embedding (2).

The internal quantum efficiency (IQE), the ratio of generated photons to the electron–hole recombinations, was increased by improving the material quality and enhancing the electron-hole recombination. Electron or hole blocking layers in multi-quantum wells (MQWs) can confine one type of carriers and enhance the electron-hole recombination, and thus increase IQE (20,21). The first generation of III- nitrides LEDs are grown on sapphire substrates and show strong polarized electroluminescence. IQE of these polar LEDs achieve over 80% at low current densities, although experience "efficiency droop" at higher drive currents (22), shown in Figure 2(a). The second generation of III-nitrides LEDs are grown on nonpolar/semipolar GaN substrates. By reducing the crystal defect in GaN substrate and the nonradiative defects in active layer of LEDs, the nonpolar/semipolar III-nitrides LEDs reduce the efficiency droop at current densities up to 400A/cm^2 (Figure 2(b)), and the output power is significantly increased at higher current densities (22).
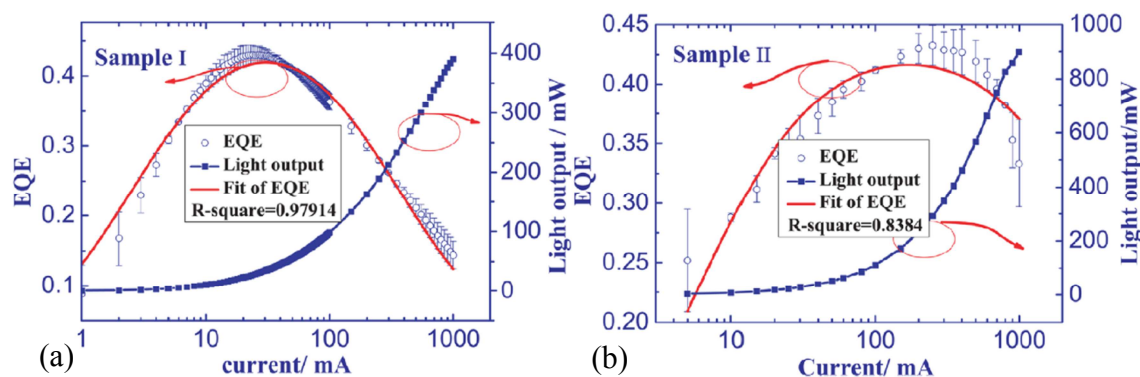

Figure 2 Quantum efficiency and light output as a function of current in (a) LED on sapphire substrate (b) LED on GaN substrate. The data points represent the measured results. The solid line on quantum efficiency represents the fitting curve based on carrier's rate equation. (22)

Bright white light LEDs are progressing due to the achievement of III-nitrides based LEDs. There are three ways of generating white light using LEDs: combination of red, green and blue LEDs, UV GaN LED plus blue and yellow phosphors, and blue III-nitrides LED with yellow phosphor. The blue III-nitrides LED with yellow phosphor dominates the white LED industry due to the simplicity of manufacturing and high theoretical efficacy (2,23).

Most white LEDs have a peak emission in the blue light range (400-490 nm) and a broad band emission around yellow light (500-700 nm). Blue light can affect many physiologic functions depending on the wavelength, intensity, duration of the exposure, and time of day. The accumulating experimental studies have indicated that LEDs with an emission peak of around 470–480 nm should not significantly increase the risk of

development of ocular pathologies, while UV light and short wavelength blue light (400-450 nm) are better to be blocked to protect the retina (24).

LEDs are used in displays for signage, outdoor video screens, television/monitor LCD backlighting, keyboards, smart phones and tablets, and they are penetrating the general illumination market. LEDs also produce a more efficient way for plant growth with a reduced carbon footprint than with traditional grow lights (25). GaN-based blue LEDs influence the exchange of CO_2 and the stoma, along with increasing anthocyanin (26,27), while green LEDs have a direct effect on stages of plant growth, such as seed dormancy and elongating the hypocotyl (27). The US Department of Energy (DOE) is driving the SSL technology development and SSL product applications; the DOE SSL program strategies predict 75% energy savings compared to the no-SSL scenario by 2035 (28).

The III-Nitrides for Solar Cells

The discovery of low-energy bandgap of 0.7 eV for InN (31, 32), as opposed to previously accepted value of 1.3 eV (33,34), has led to its wide use in conjunction with GaN (35-37). Due to InGaN's tunable bandgap from 0.7 eV (InN) to 3.4 eV (GaN), covering the entire air-mass-1.5 solar spectrum, it has been known as a candidate for high efficiency multi-junction photovoltaic devices. In a theoretical analysis, it was demonstrated for an InGaN-based four-junction solar cell to obtain power conversion efficiency (PCE) greater than 50%, In content of about 40% is required (38).

InGaN alloys have superior high energy radiation resistance, which can be used in space-based photovoltaic applications (39). Absorption coefficients in the order of 10^5 cm^{-1} have been obtained at the band edges of grown GaN and InGaN samples (40). This indicates more than 99% of the incident light with energy higher than the bandgap is absorbed within the first 500 nm of the material, leading to fabrication of relatively thin solar cell structures.
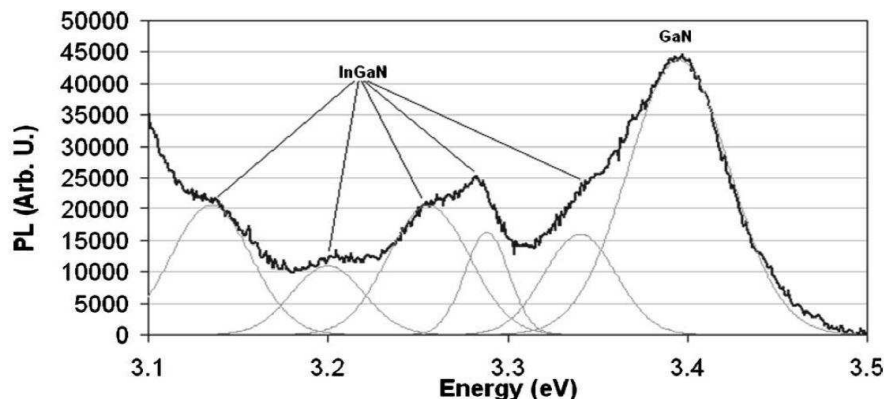

Figure 3 RT photoluminescence of MOCVD-grown GaN/InGaN solar cell indicating an apparent phase separation in InGaN (41).

Work done by Jani et al. (41) is among the first endeavors to experimentally demonstrate GaN as a high performance photovoltaic material. A p-i-n heterojunction structure, with $In_xGa_{1-x}N$ (x: 4-5%) as the active material with thickness of 200 nm, and GaN as the p- and n- contacts, was fabricated using MOCVD. Phase separation within the

material, observed through room temperature (RT) photoluminescence, was the primary challenge during the epitaxial growth as shown in Figure 3. It was observed that the lower bandgap phase-separated material leads to deterioration of open-circuit voltage (V_{oc}) and short-circuit current density (J_{sc}). The problem of phase separation was later resolved through improved processing steps due to advancement of growing InGaN alloys using MOCVD (42).

Growing InGaN epilayers on GaN beyond a critical thickness causes extended crystalline defects in the InGaN epilayer close to the InGaN/GaN interface (43), primarily due to the large lattice mismatch between InN and GaN. The critical thickness of active layers in a p:$In_{0.175}Ga_{0.835}N$/n-$In_{0.16}Ga_{0.84}N$ homo-junction was shown to be limited to 60 nm and 45 nm, respectively (44). This value reduces significantly by increasing the In alloy content, to about 1 nm for $In_{0.2}Ga_{0.8}N$ (45), leading to the partial loss of incident light due to transmission through the device. XRD and I-V measurements shows degradation of electrical characteristics and crystal quality of a MOCVD-grown 24 nm InGaN layer by increasing the In content from 30% to 40% (42).

Table I. Electrical characteristics of GaN-based solar cells

Structure	In Content (%)	V_{oc} (V)	J_{sc} (mA/cm^2)	Ref.(Yr.)
p:GaN/i:InGaN/n:GaN	4-5	2.40	4.00	41 (2007)
p:GaN/i:InGaN/n:GaN	10	2.09	0.52	46 (2009)
p:GaN/i:InGaN/n:GaN	12	1.81	4.20	47 (2008)
p:GaN/i:InGaN/n:GaN	12	1.89	1.06	48 (2011)
i:InGaN/NID*:GaN	6.2	1.04	0.57	49 (2017)
p:InGaN/n:GaN	17	1.47	0.26	50 (2010)
InGaN/GaN MQW*	20	2.26	2.10	52 (2016)
InGaN/GaN MQW	30	2.00	1.50	42 (2009)
InGaN/GaN MQW	30	1.95	0.83	33 (2010)
InGaN/GaN MQW	30	2.01	0.97	34 (2016)
InGaN/GaN MQW	35	1.80	2.56	35 (2010)
InGaN QD*/GaN SL*	10	0.7	1.38	36 (2014)
InGaN/InGaN SL	17	1.78	3.08	37 (2011)
PEDOT:PSS/GaN	-	0.331	13.7	38 (2016)
NiAu/InGaN Schottky	10	0.40	0.065	39 (2016)

*NID: Not-intentionally doped   *QD: Quantum dot
*MQW: Multiple quantum wells   *SL: Superlattice

The electrical characteristics of several fabricated GaN-based solar cells are reported in Table 1 and sorted in order of device structure as well as In composition level. As shown, by increasing the In alloy content, the V_{oc} and J_{sc} are degraded in most of the device structures. This indicates most of the research work done in this field used In alloy content of maximum 35%.

Recently, metal-semiconductor (M-S) junction has been used to alleviate the problem of p-type doping in GaN and InGaN layers, in which the rectifying Schottky junction between NiAu and InGaN causes the photo-generated current to flow throughout the fabricated device (38). However, considerable work needs to be done for improving the performance of such Schottky solar cells.

Therefore, GaN and its alloy InGaN, have shown promising results for the photovoltaic applications due to their tunable direct bandgap throughout all levels of In composition and high absorption coefficient. However, the degradation of crystal quality

and electrical characteristics by increasing the In level, in addition to very thin critical thickness for avoiding the defects, have restricted fabrication of high efficiency solar cells based on GaN. Advancements have been done to eliminate these limitations, either by using multiple quantum wells, superlattices, or Schottky junctions, but there still exists a need for further investigation and improvement in the characteristics of the solar cells.

The III-Nitrides for High Power Electronics and RF application

GaN is recognized as a forerunner in electronics applications due to its high band gap (3.4 eV), breakdown voltage above 200 V, power density above 10.3 W/mm, and electron mobility greater than 1250 cm^2/Vs (60-63). Wide bandgap devices can potentially replace silicon technology currently facing challenges to sustain Moore's law due to its limitations in heat dissipation, power consumption, switching speed, high voltage, and high temperature. GaN can potentially operate at high voltage, high frequency, and high temperature. GaN usage was initiated from LED and is now an emerging material for power electronics. Extensive research is currently being conducted to reduce the cost of GaN and allied devices for higher efficiency application in converters, inverters and rectifiers.

GaN also assures to meet the future demand of high signal bandwidth for faster communication, in addition to a large amount of data consumption. As compared to silicon devices, GaN-based devices possess higher frequency range operation (18 GHz and greater), and improved power amplifier efficiency (PAE) (25% and greater). GaN-based high electron mobility transistors (HEMT) devices and monolithic microwave integrated circuits (MMIC) promise to play the leading role for the future devices.

GaN application in high power electronics

Improvement in power converters efficiency and reduction of size and cost has been one of the current research areas in GaN. GaN Schottky devices are now available in the range of 600-3.3 kV manufactured using hydride vapor phase epitaxy method (61). GaN devices are also getting more attention due to the lower specific on-resistance of and higher breakdown voltage compared to Si devices (64). Research on GaN heterojunction field effect transistors (HFET) illustrates the larger the layer of epitaxial growth, the larger the breakdown voltage. Breakdown voltage of 2000 V was reported for the epitaxial growth layer of 6.5 μm (63). GaN devices have shown higher competencies over the silicon MOSFET devices in DC-DC converters application. GaN and allied compounds are being used in Buck and Boost converters. Efficient boost converters in the voltage range of 175-350 V (efficiency of 97.8% and output power of 300 W) and at 940 V (efficiency of 94.2% and output power of 122 W) are reported for 1 MHz switching frequency (65-67). Boost converters Comparison between GaN FET-based and Si MOSFET-based 48/12 V unregulated isolated bus converters at 1.2 MHz, show that power loss in GaN FET device was 25% less than the Si MOSFET device (64) . This demonstrates the capability of GaN for high efficiency application in boost converter. GaN HEMT devices application is also studied for 300 W, hard-switching 400/12 V buck converter. This paper has confirmed that the efficiency of GaN HEMT devices is higher at light load compared to Si MOSFET (68).

A recent research study on Schottky diode grown using MOCVD indicated that leakage current is controlled and reverse breakdown voltage of 200 V (69). Though the conversion and charge collection efficiencies are estimated about 0.32% and 29% or less respectively, improved quality of GaN films will improve the performance of Schottky diodes. This in turn can be used in GaN betavoltaic nuclear batteries (GNBB). Satisfactory results were obtained for Schottky diode at temperature higher than 200°C with a breakdown voltage higher than 1000 V. A very short recovery time of 10 ps makes this device more suitable for high switching frequency operation (70).

GaN role in RF application

Advancement due to 2D electron-gas interface between AIGaN and GaN with high electron mobility range, in the range of 1200 cm^2/Vs to 2000 cm^2/Vs, has increased the power capability of HEMT devices from 1.1 W/mm in 1996 to 40 W/mm presently (61). GaN nanowire can serve as fundamental structure for the assembly of nanodevices with an electron mobility close to 650 cm^2/Vs. Recent development of HEMT device is focused in normally-off mode, emphasizing more on gate structures. HEMT with a breakdown voltage of 8.3 kV has been developed using GaN on a sapphire substrate (61). GaN/AlGaN heterojunctions with high current gain cut-off frequency of 153 GHz and power gain cut-off frequency of 198 GHz with a gate length of 100 nm have been reported. A combination of n-type GaN devices and p-type Si devices can impart good rectifying characteristics, generating the opportunity for complex and nanoscale optoelectronic system (71). Non-uniform distributed topology based GaN MMIC power amplifiers has been reported having remarkable average output power of 6 W and efficiency of 29.5 % with frequency range of 2 – 18 GHz (72).

Thus, GaN is emerging as a promising device for high power and RF applications owing to its characteristics such as high breakdown voltage, high power densities, and high electron mobility. However, there are challenges related to HEMT gate design, high cost, and lack of switching testing devices for GaN which are yet to be addressed. Further investigation on fabrication techniques and a substrate study is also required to realize the full potential of GaN devices.

The III-Nitrides for Magnetic Applications

The versatility of GaN as a dilute magnetic semiconductor (DMS) stems from the possibility of doping GaN with transition metals (TM) and rare-earth metals (RE) to achieve room temperature ferromagnetism. Combining the magnetic moments of electrons in partially filled d orbital of TM, or d and f orbitals of RE metals, with the semiconducting and optical properties of established GaN has arisen interest in GaN for spintronic applications as explained further.

Theoretical analysis based on Zener's ferromagnetism predicted the existence of RT ferromagnetism in GaMnN with 5% Mn and 3.5 x 10^{20} holes/cm^3(73). Small lattice constant and presence of nitride anion in GaN, doped with Mn containing a half-filled d orbital result in this ferromagnetism. Local spin density calculations show that magnetic TM-doped DMS forms deep levels in GaN, and that the Curie temperature (T_c) initially increases with an increase in the TM concentration but at high concentrations, the T_c

decreases due to the formation of TM clusters (74). These clusters have antiferromagnetic TM-N and ferromagnetic TM-TM coupling (75). A magnetic moment ranging from 4 μ_b to 22 μ_b per Mn-N cluster was theoretically predicted (76). However, this was not in coherence with the experimental results reported. Saturation magnetization of 2.4 µB/Mn atom was observed in MOCVD-grown 1% doped GaMnN sample as measured by SQUID (superconducting quantum interference device) magnetometry (77). Annealing reduced the magnetization due to the formation of phases that do not contribute to ferromagnetism. Si codoping compensates the Mn acceptors that substitute Ga. Additionally, Si codoping and annealing increase the Fermi level resulting in nitrogen vacancies and trapped donor electrons.

Similar behavior of RT ferromagnetism was observed in GaFeN with 0.7% Fe doping grown using MOCVD, except that no change is observed with Si codoping (78). The effect of thickness of Fe films on the Fe/GaN interface roughness and on the resulting ferromagnetic behavior was investigated by growing Fe films using MBE on MOCVD-grown GaN on sapphire (79). An increase in roughness at the GaN/Fe interface was observed with an increase in the Fe layer thickness up to 10 nm, which resulted in enhanced coercivity and saturation magnetization. Moment of 2.18 μ_B/atom was observed for samples with Fe layers with thickness over 5 nm, measured using SQUID, vibrating sample magnetometer (VSM) and polarized neutron reflectometry. GaCrN, is another TM doped DMS that showed RT ferromagnetism of 15 emu/cm^3 and 2.26 μ_B per Cr atom, grown using radio-frequency plasma-assisted MBE on sapphire substrates (80). On doping the samples with Si, crystal quality was improved and magnetization was reduced. Long-range mediation between Cr, Si and V_{Ga} is considered responsible for this behavior. While clustering, defects and other carrier mediated mechanisms potentially explain the observed ferromagnetic behaviors in TM doped GaN, further work is needed to ascertain the mechanisms at varying doping levels of TM.

Elements such as Gd, Er, Eu, Sm and Nd have been doped in GaN with intent to analyze the optical, electrical and magnetic properties (81-87). Gd has been the most explored rare-earth dopant with half-filled f and partially filled d orbitals. GaGdN can be doped with donors or acceptors with a density more than that of Gd to introduce additional spin-polarized carriers. Room temperature ferromagnetism in the order of 1000 µB per Gd atom was achieved in GaGdN grown using ammonia-assisted MBE on SiC and doped with low Gd concentration of 10^{16} cm^{-3} (81,89). This gave an impetus for further theoretical and experimental analysis of ferromagnetism in GaGdN. As the GaGdN samples were insulating, the observed colossal magnetic moment is not carrier mediated. The samples contained oxygen in the order of 10^{18} cm^{-3}, which possibly resulted in p-d hybridization and contributed to the magnetic moment of the sample. In another study, MOCVD grown GaN was doped with Gd from two sources, from ((TMHD)$_3$Gd) that has oxygen in its organic ligand, and (Cp$_3$Gd) that does not contain oxygen (81). RT ferromagnetism was observed only in samples with oxygen-containing Gd source. Magnetization in GaGdN has been enhanced by codoping with Si and Mg. Annealed p-type Ga$_{0.98}$Gd$_{0.02}$N samples exhibited magnetization up to 500 emu/cm^3,while a maximum magnetization of 110 emu/cm^3 was observed in n-type Ga$_{0.98}$Gd$_{0.02}$N (81). VSM measurements of p-doped GaGdN are shown in Figure 4. Holes are considered to be more dominant than electrons in contributing to the ferromagnetism in GaGdN. First principle calculations of Mg doped nanowires predict lattice distortions when Mg substitutes Ga (89). Also, codoping with C is predicted to increase magnetization in

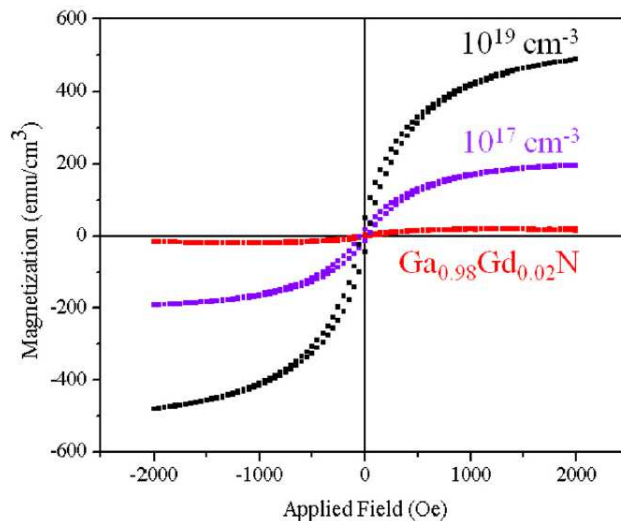GaGdN as per Zeners' p-d exchange mechanism (90).

Figure 4. RT VSM measurements of p-doped GaGdN (81)

Ga vacancies also contribute to the observed ferromagnetism in GaGdN and GaN. Ga vacancies were intentionally introduced by annealing GaN samples at high temperatures ranging from 800 $^\circ$C to 1000 $^\circ$C, grown using laser MBE on sapphire (91,92). Magnetization up to 2.67 emu/cm^3 was observed in a GaN sample with a ratio of N to Ga of 1.52. Ga vacancies could possibly contribute to ferromagnetism in TM and RE doped GaN, but act as a primary mechanism in unintentionally doped GaN.

Thus, GaN-based compounds have been explored for magnetic behavior and have the potential for use in spintronic applications. Although several theories and mechanisms have been proposed to explain ferromagnetism in TM and RE doped GaN and experiments are performed, further work is necessary to understand the origin of magnetism in GaN-based materials and for reproducibility of the results.

The III-Nitrides for Thermoelectric Energy Harvesting

The III-Nitride materials exhibit an intrinsically high Seebeck coefficient and excellent temperature stability in their electrical properties due to their wide bandgaps (93). This makes them a good candidate for high temperature thermoelectric (TE) electricity generation from waste energy harvesting. In particular, the low ionization of p-type dopants of 2-3% seen at room temperature will increase at higher temperatures with a corresponding improvement in TE device performance. SiGe TE materials and devices peak around 900 K due to the bipolar effect so III-Nitride devices would be a desirable alternative at higher temperatures (93).

Thermoelectric (TE) devices can directly convert waste heat into electrical power, which has a significant potential to impact renewable energy technologies, as nearly 60% of energy produced in US is lost as a form of heat each year (94). A significant portion of waste heat, 20%-50%, is generated from high temperature industrial processes, such as power plants, metal furnaces, and chemical production. However, most of the common TE materials are narrow bandgap materials that are often toxic and rare (i.e., BiTe, PbTe). Therefore, their applications are hindered by low operational temperature, high

cost and toxicity (93). While many new materials and novel device structures have been investigated for TE applications, few of them offer the temperature stability of the III-Nitride materials, and can benefit from a pre-existing device technology.

GaN is one of a new generation of semiconductors that is attracting interest for TE applications (95). GaN most commonly has a wurtzite crystal structure or sometimes zinc blende structure. TE properties of GaN materials grown by different deposition techniques have been reported by various research groups. The highest absolute value of Seebeck coefficient for thin film GaN is around 500 µV/K and this occurs at low carrier concentrations (96). The optimization of TE materials requires the decoupling of the electrical and thermal properties of the material to give the highest value of the figure of merit, ZT. One approach has been the use of InN/GaN nanowire structures which have a higher electrical conductivity and lower thermal conductivity than that of GaN. As such, a ZT of ~0.86 was reported for these nanostructures with a carrier concentration of $7x10^{17}$ cm^{-3} at 300 K, and the estimated ZT is likely to reach 1.71 at 1000 K (97).

Fabrication of GaN-based TE device structures ranging from centimeter-size to sub-millimeter size dimensions have been reported. These devices could then be measured under load to evaluate actual operational characteristics of the device, rather than the estimated performance indicated by the value of ZT. These were typically multi-junction hybrid devices that were constructed from free-standing or epitaxial hydride vapor phase epitaxy (HVPE) grown GaN (98,99). For example, a 3-pair epitaxial GaN layers device structure was fabricated for the purpose of on-chip integration (100). In these prototypes of devices chromel was sputtered onto the SiO_2 glass substrate and then the GaN was physically soldered on. In a later study, an integrated GaN-based lateral TE device was grown by MOCVD. This device used more traditional device fabrication processes to produce thermally stable Ti/Al/Ni/Au ohmic contacts with Ti/Au interconnects to achieve p–n pairs (98). It is observed that both V_{op} and P_{max} increase linearly with the number of p-n pairs, 1, 5, 10 and 25 pairs, and V_{op} reaches a maximum of 0.3 V for the 25 elements device with a P_{max} of 2.1 µW at $\Delta T=30K$ and $T_{avg} =508$ K.

AlN (6.2 eV) and InN (0.7eV) have also been considered for TE devices, but less work has been done for these materials compared to GaN. This is due to the difficulty of doping AlN and growing InN. An investigation of the phonon transport of AlN found that the average mean free path of phonon in the zinc-blende phase is roughly four times that of in the wurtzite phase (101). This indicates that AlN has a significantly higher thermal conductivity in the zinc-blende phase, which implies that the wurtzite phase is better suited for TE applications in high temperature applications. InN is promising for TE applications since the large size of indium atoms potentially increases phonon scattering and accordingly reduce the thermal conductivity (98). The highest reported ZT is about 1.6 for a 6 nm InN nanowire at 1000 K, which is 100 times larger than that at room temperature (102). Hybrid, InN and $Al_{0.25}In_{0.75}N$ devices structures prepared by radio-frequency (RF) sputtering have been fabricated (103). However, a device composed of 20-pair elements pairs did not show an improvement over that reported for GaN.

Recent work has focused on the alloys of the III-Nitrides, especially InGaN and AlGaN, due to ability to potentially decouple the electrical and thermal properties of layered structures. InGaN material has been investigated at various compositions at room temperature (104,105). A negative correlation has typically been observed between

Seebeck coefficient and InN fraction. However, the TE quality of materials depends heavily on how the material was grown and its homogeneity. For instance, InGaN tends to show phase separation at relatively low indium concentrations, if this is properly controlled, high values of ZT can be seen for the InN fraction is below 0.2. The optimal indium content appears to be 0.2 with a resulting ZT of 0.04 (104) and 0.072 (105) have been reported at room temperature. Most studies on $Al_xGa_{1-x}N$ investigate the effect of the mass fraction of aluminum, x, or the carrier density, n, on the TE properties and their associated ZT value (106,107). The results show that the higher mass fractions of Al often result in lower thermal conductivities, and thermal conductivity decreases with the increase of temperature due to increased phonon scattering. A recent study has explored a way to modify the ZT value for $Al_{0.2}Ga_{0.8}N$ by achieving high electrical conductivity and low thermal conductivity. This is done by polarizing the electrical field of the $GaN/AlN/Al_{0.2}Ga_{0.8}N$ superlattices, leading to a much higher electron mobility, increasing the ZT value to 0.08 at room temperature (108). The future promise of III-Nitride for TE applications can be seen in Figure 5 which shows the variation of Seebeck coefficient for various binary materials and alloys.
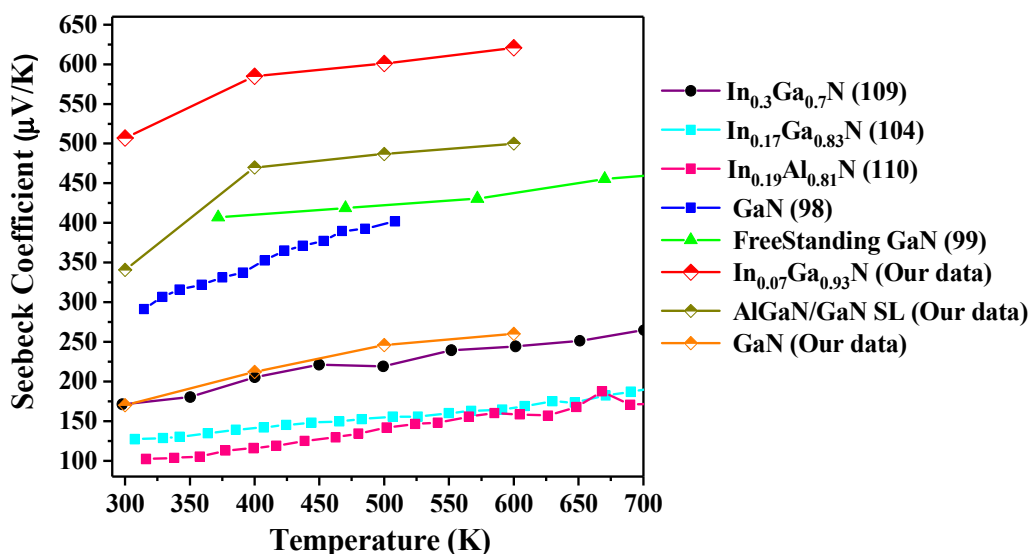

Figure 5 Temperature dependent Seebeck coefficient for various binary materials and alloys

III-Nitrides for Nuclear Detection

The current state of the art in detection of thermal neutrons is the gas-filled proportional counter, and for gamma radiation detection it is the high purity germanium detector (111). Gas-filled counters are expensive, bulky, fragile, and require very high voltages to operate. High purity germanium detectors are also bulky because they are operated at liquid nitrogen temperatures. A solution to these issues is the use of compound semiconductor materials such as the III-Nitrides which can offer detection technology that is more cost-effective and more rugged than current systems (112). GaN can be utilized as either scintillation material or as a semiconductor detector for either thermal neutrons or gamma radiation (113). GaN is a novel material for these applications but has many favorable properties as appropriate dopants can be incorporated to enhance their sensitivity to radiation. The most common dopant elements to create radiation detecting

materials are In, Gd, B, and Li. Indium is of interest in gamma scintillators because of its high Z number. Gd, B, and Li are beneficial for neutron scintillators and semiconductor thermal neutron detectors because of their large charged particle production cross section. Techniques for doping, control of conductivity type, and bandgap engineering are well understood in GaN-based materials and optimized detectors can be thin enough to provide built-in gamma discrimination. One significant benefit of GaN-based materials for radiation detectors is the mature, radiation hard, device technology that already exists for GaN-based electronics and optoelectronics into which detectors can be integrated.

The incorporation of indium into GaN is exceptionally mature technology and homogenous layers of InGaN can be obtained for compositions of 25-30% (115). Indium is favored for neutron scintillation detectors in GaN thin films because of its high Z number. However, indium is not always good in neutron detectors since it also an alpha detector which takes long lifetimes for recovery after sensing this source of radiation. Gadolinium is also of interest in GaN thin films because of its high Z number and its extremely high cross-section for thermal neutron detection of ~250,000 barns (116). Gd behaves as a stable center in GaN, substituting for a Ga atom, and has primarily been investigated for spintronic applications. Room temperature ferromagnetism has been reported in Gd-doped GaN thin films with very large magnetic moments. Gd-doped GaN often shows optical transitions characteristic of the d→f intra-subband transitions in Gd, which have higher energies than the GaN bandgap and the effect of thermal neutrons on these transitions still needs to be investigated. The nature of incorporation of Gd in GaN is still unclear and how it may influence neutron detection. Boron has also been investigated in GaN for use in high electron mobility transistors, UV optoelectronics and thermal neutron detection (117). Boron, like indium, is a group III element which forms an intrinsic alloy with GaN. BGaN thin films have been grown by MOCVD with ~1.4% boron.   However, although boron forms an intrinsic alloy with GaN at low concentrations, boron nitride is a cubic material and begins to phase separate at higher boron concentrations. Therefore, the effects of boron concentration on material quality and subsequent detector performance are not well known.   The use of lithium as dopant with semiconductor materials should be avoided (118). Lithium is a fast diffuser in most compound semiconductor materials and typically shorts out any p-n junction within the device. Gadolinium would always be favored as its cross section is a factor of 1000 greater than lithium, and it can be used in its natural form.

GaN is ideal for neutron scintillation work as single crystal devices can be grown (118). GaN can be heavily doped to produce ultra-fast, non-hygroscopic, dense, highly sensitive neutron or photon scintillators. High dopant levels of Li-6 and B-10 have already been incorporated onto these substrate crystals allowing variable scintillation wavelengths with various decay times. The tunable emission is useful in the optimization of these structure for matching with the light collection device. This detector design can also be inherently blind to photon events.   Thermal neutron scintillation detectors composed of GaN thin films via the ^{14}N(n, p) reaction have been investigated, Figure 6 (119). Pulse-height gamma discrimination was shown to be possible with a neutron-to-gamma ratio of 78:1. In addition, GaN-based scintillation detectors were found to have a linear response to nuclear reactor power level over more than two orders of magnitude. This indicates that these materials may be a suitable neutron detection technology in high-flux applications such as reactor monitoring.
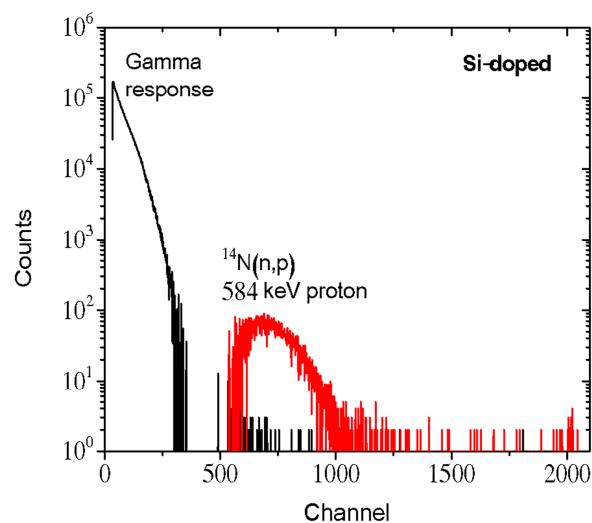
Figure 6 Gamma and thermal neutron scintillation spectra produced by bare Si-doped GaN scintillator

Several thermal neutron detectors have been reported that use a "conversion layer" rich in high cross-section elements (usually B or Li) which has been deposited on top of a p-n semiconductor diode. Neutrons react in the conversion layer producing charged particles that excite electrons in the diode which are then collected by applying an external bias. These devices are limited in potential efficiency, however, because many of the charged particles produced by the neutron reactions in the conversion layer are either reabsorbed by the conversion material or are directed away from the diode (120). Thermal neutron detector devices can be GaN diodes of p-n or p-i-n type, with an active region between the p- and n-type layers. As discussed before, these active regions will consist of GaN doped with Gd, B, or Li. Doping with B or Li will utilize their respective (n,α) reactions to generate electron-hole pairs, while Gd will produce Auger electrons that can be used in the same way (121). Rather than allowing these carriers to recombine (as in the scintillators), these devices can be reverse biased to collect the electrons and holes, resulting in a signal current.

III-Nitrides for Other Novel Applications

Photoelectrochemical Water Splitting

Photoelectrochemical water splitting has attracted considerable attention for sustainable energies. Photocatalyst materials absorb solar energy to generate hydrogen, a carbon-free and sustainable energy source. InGaN alloy has been developed recently for solar-hydrogen production due to ites tunable bandgap across almost the entire solar spectrum, and the conduction and valence band edges of InGaN that can straddle water oxidation and hydrogen redox potentials. InGaN/GaN nanowires and nanosheets with large surface-to-volume ratios have been investigated to enhance the charge carrier separation, surface reaction, and therefore the conversion efficiency. (122-124)

Photonic and Plasmonic

Nanostructure arrays, such as nanowires, nanocones, nanospheres and nanoparticles, can form photonic resonant modes, such as a gradient of effective refractive index, leading to confinement and absorption of light. Plasmonic resonance corresponds to the incident photon excited collective oscillations of electrons. Plasmonic nanostructures can lead to localized plasmonic resonance and enhancement in light emission (126). Plasmonic nanoparticles have been proven to increase light scattering, light trapping, and carrier collection in InGaN solar cells, leading to enhancement of its external quantum efficiency (127). On the other hand, nanoparticles or photonic crystals with proper size and array on LED surface can enhance both the Purcell spontaneous emission from the nitrides into the surface nanostructures, and radiation modes coupling from the nanostructures outward to the air, leading to enhancement of the light emission efficiency of LEDs (128,129).

Conclusion

III-nitrides are universal compound semiconductors in various application fields due to their exceptional properties in energy band, electrical transport, magnetic and thermoelectric. III-nitrides applications in LEDs contribute to revolutionary progress in solid state lighting. The III-nitride solar cells and thermoelectric development are essential for the sustainable and renewable energy economy and society. Novel devices in power and RF electronics, spintronic applications and nuclear detections are developing extensively and will play important roles in the field. The investigation on III-nitrides material growth, property study, device design and fabrication will lead to more stable, affordable, and applicable technologies.

Acknowledgments

References

1. M. O. Manasreh, I.T. Ferguson, *III-nitride Semiconductor: Growth*, Taylor & Francis (2003).
2. E. Fred Schubert, *Light-Emitting Diodes*, chapter 12, Cambridge University Press (2006).
3. S. Nakamura and M. R. Krames, *Proceedings of the IEEE*, **101**, 2211 (2013).
4. S. P. DenBaars, D. Feezell, K. Kelchner, S. Pimputkar, C.C. Pan, C.C. Yen, S. Tanaka, Y. Zhao, N. Pfaff, R. Farrell, M. Iza, S. Keller, U. K. Mishra, J. S. Speck, S. Nakamura, *Acta Materialia*, **61**, 945 (2013).
5. D. Zhu, D.J, Wallis and C. J. Humphreys, *Rep. Prog. Phys.*, **76**, 106501(2013).
6. J.I. Pankove, E.A. Miller and J.E. Berkeyheiser, *RCA Review*, **32**, 383 (1971).
7. S. Yoshida, S. Misawa, and S. Gonda, *Appl. Phys. Lett.*, **42**, 427 (1983).
8. H. Amano, N. Sawaki, I. Akasaki, and Y. Toyoda, *Appl. Phys. Lett.*, **48**, 353 (1986).
9. S. Nakamura, *Jpn. J. Appl. Phys.*, **30**, L1705, (1991).
10. H. Amano, M. Kito, K. Hiramatsu, and I. Akasaki, *Jpn. J. Appl. Phys.*, **28**, L2112 (1989)

11. S. Nakamura, T. Mukai, M. Senoh, and N. Iwasa, *Jpn. J. Appl. Phys.*, **31**, L139 (1992).
12. S. Nakamura, T. Mukai, and M. Senoh, *Jpn. J. Appl. Phys.*, **30**, L1998 (1991).
13. S. Nakamura, M. Senoh, and T. Mukai, *Jpn. J. Appl. Phys.*, **32**, L8 (1993).
14. S. Nakamura, T. Mukai, and M. Senoh, *Appl. Phys. Lett.*, **64**, 1687 (1994).
15. S. Nakamura, M. Senoh, N. Iwasa, and S. Nagahama, *Jpn. J. Appl. Phys.*, **34**, L797 (1995).
16. S. Nakamura, M. Senoh, N. Iwasa, S. Nagahama, T. Yamada, and T. Mukai, *Jpn. J. Appl. Phys.*, **34**, L1332 (1995).
17. M. Pophristic, F. H. Long, C. Tran, I. T. Ferguson, and R. F. Karlicek Jr., *Appl. Phys. Lett.*, **73**, 3550 (1998).
18. E. Park, J. Jang, S. Gupta, I. Ferguson, C. Kim, S. Jeon, and J. Park, *Appl. Phys. Lett.*, **93**, 191103 (2008).
19. M. R. Krames, O. B. Shchekin, R. M.-Mach, G. O. Mueller, L. Zhou, G. Harbers, and M. G. Craford, *IEEE J. Display Technol.*, **3**, 160 (2007).
20. Y. Narukawa, M. Ichikawa, D. Sanga, M. Sano, and T. Mukai, *J. Phys. D, Appl. Phys.*, **43**, 354002 (2010).
21. E. Park and I. T. Ferguson, S. Jeon, J. Park, and T. Yoo, *Appl. Phys. Lett.*, **89**, 251106 (2006).
22. E. Park, D. Nicol, H. Kang, I. T. Ferguson, S. Jeon, J. Park and T. Yoo, *Appl. Phys. Lett.*, **90**, 031102 (2007).
23. Z. Liu, J. Ma, X. Yi, E. Guo, L. Wang, J. Wang, N. Lu, J. Li, I. Ferguson, A. Melton, *Appl. Phys. Lett.* **101**, 261106 (2012).
24. Z. Liu, T. Wei, E. Guo, X. Yi, L. Wang, J. Wang, G. Wang, Y. Shi, I. Ferguson, and J. Li, *Appl. Phys. Lett.*, **99**, 091104 (2011).
25. S. Nakamura and G. Fasol, The Blue Laser Diode. Berlin, Germany: Springer-Verlag, 216 (1997).
26. G. Tosini, I. Ferguson, K. Tsubota, *Molecular Vision*, **22**, 61 (2016).
27. R.J. Bula, R.C. Morrow, T.W. Tibbitts, D.J. Barta, R.W. Ignatius, and T.S. Martin, *HortScience*, **26**, 203 (1991).
28. G. D. Massa, H. Kim, R. M. Wheeler, and C. A. Mitchell, *Hort Science* 43 (2008).
29. Y. Wang and K. M. Folta, *American Journal of Botany*, **100**, 70 (2013).
30. DOE Solid-State Lighting Program -- Modest Investments, Extraordinary Impacts (2017).
31. S. Nakamura, S. Pearton, and G. Fasol, *The Blue Laser Diode*, Springer-Verlag, Berlin, 216 (2000).
32. J. Wu, W. Walukiewicz, K. M. Yu, J. W. Ager III, E. E. Haller, H. Lu, W. J. Schaff, Y. Saito, and Y. Nanishi, *Appl. Phys. Lett.*, **80**(21), 3967 (2002).
33. T. Inushima, V. V. Mamutin, V. A. Vekshin, S. V. Ivanov, T. Sakon, M. Motokawa, and S. Ohoya, *J. Cryst. Growth*, **227**, 481 (2001).
34. J. Wu, W. Walukiewicz, K. M. Yu, J. W. Ager III, E. E. Haller, H. Lu, and W. J. Schaff, *Appl. Phys. Lett.*, **80**(25), 4741 (2002).
35. V. Y. Davydov, A. A. Klochikhin, V. V. Emtsev, S. V. Ivanov, V. V. Vekshin, F. Bechstedt, J. Furthmuller, H. Harima, A. V. Mudryi, A. Hashimoto, A. Yamamato, J. Aderhold, J. Graul, and E. E. Haller, *Phys. Stat. Sol. (B)*, **230**(2), R4 (2002).
36. T. M. Smeeton, M. J. Kappers, J. S. Barnard, M. E. Vickers, and C. J. Humphreys, *Appl. Phys. Lett.*, **83**(26), 5419 (2003).

37. Y. C. Shen, G. O. Mueller, S. Watanabe, N. F. Gardner, A. Munkholm, and M. R. Krames, *Appl. Phys. Lett.*, **91**(14), 141101 (2007).

38. A. de Vos, *Endoreversible Thermodynamics of Solar Energy Conversion*, p. 90, Oxford University Press, Oxford, UK (1992).

39. J. Wu, W. Walukiewicz, K. M. Yu, W. Shan, J. W. Ager III, E. E. Haller, H. Lu, W. J. Schadd, W. K. Metzger, S. Kurtz, *J. Appl. Phys.*, **94**(10), 6477 (2003).

40. J. F. Muth, J. H. Lee, I. K. Shmagin, R. M. Kolbas, H. C. Casey Jr, B. P. Keller, U. K. Mishra, and S. P. DenBaars, *Appl. Phys. Lett.*, **71**(18), 2572 (1997).

41. O. Jani, I. T. Ferguson, C. Honsberg, S. Kurtz, *Appl. Phys. Lett.*, **91**(13), 132117 (2007).

42. R. Dahal, B. Pantha, J. Li, J. Y. Lin, and H. X. Jiang, *Appl. Phys. Lett.*, **94**(6), 063505 (2009).

43. N. Faleev, B. R. Jampana, O. Jani, H. Yu, R. Opila, I. T. Ferguson, and C. Honsberg, *Appl. Phys. Lett.*, **95**(5), 051915, (2009).

44. B. R. Jampana, A. G. Melton, M. Jamil, N. N. Faleev, R. L. Opila, I. T. Ferguson, and C. B. Honsberg, *IEEE Electron Dev. Lett.*, **31**(1), 32 (2010).

45. D. Holec, Y. Zhang, D. V. S. Rao, M. J. Kappers, C. McAleese, and C. J. Humphreys, *J. Appl. Phys.*, **104**(12), 123514 (2008).

46. R. Dahal, B. Pantha, J. Li, J. Y. Lin, and H. X. Jiang, *Appl. Phys. Lett.*, **94**(6), 063505 (2009).

47. R. H. Horng, S. T. Lin, Y. L. Tsai, M. T. Chu, W. Y. Liao, M. H. Wu, R. M. Ling, and Y. C. Lu, *IEEE Electron Dev. Lett.*, **30**(7), 724 (2009).

48. C. J. Neufeld, N. G. Toledo, S. C. Cruz, M. Iza, S. P. DenBaards, and U. K. Mishra, *Appl. Phys. Lett.*, **93**(14), 143502 (2008).

49. E. Matioli, C. Neufeld, M. Iza, S. C. Cruz, A. A. Al-Heji, X. Chen, R. M. Farrell, S. Keller, S. DenBaars, U. K. Mishra, S. Nakamura, J.Speck, and C.Weisbuch, *Appl. Phys. Lett.*, **98**(2), 021102 (2011).

50. M. Arif, W. Elhuni, J. Streque, S. Sundaram, S. Belahsene, Y. E. Gmili, M. Jordan, X. Li, G. Patriarche, A. Slaouif A. Migan, R. Abderrahimd, Z. Djebbour, P. L. Voss, J.P.Salvestrini, A.Ougazzaden, *Sol. Energ. Mat. Sol. Cells*, **159**, 405 (2017).

51. B. R. Jampana, A. G. Melton, M. Jamil, N. N. Faleev, R. L. Opila, I. T. Ferguson, C. B. Honsberg, *IEEE Electron Dev. Lett.*, **31**(1), 32 (2010).

52. N. G. Young, R. M. Farrell, Y. L. Hu, Y. Terao, M. Iza, S. Kellet, S. P. DenBaards, S. Nakamura, *Appl. Phys. Lett.*, **103**(17), 173903 (2013).

53. K. Y. Lai, G. J. Lin, Y. L. Lai, Y. F. Chen, J. H. He, *Appl. Phys. Lett.*, **96**(8), 081103 (2010).

54. Z. Chen, X. Zheng, Z. Li, P. Wang, X. Rong, T. Wang, X. Yang, F. Xu, Z. Qin, W. Ge, B. Shen, and X. Wang, *Appl. Phys. Lett.*, **109**(6), 062104 (2016).

55. R. Dahal, J. Li, K. Aryal, J. Y. Lin, and H. X. Jiang, *Appl. Phys. Lett.*, **97**(7), 073115 (2010).

56. L. Sang, M. Liao, Q. Liang, M. Takeguchi, B. Dierre, B. Shen, T. Sekiguchi, Y. Koide, and M. Sumiya, *Adv. Mater.*, **26**(9), 1414 (2014).

57. Y. Kuwahara, T. Fujii, T. Sugiyama, D. Iida, Y. Isobe, Y. Fujiyama, Y. Morita, M. Iwaya, T. Takeuchi, S. Kamiyama, I. Akasaki, and H. Amano, *Appl. Phys. Express*, **4**(2), 021001 (2011).

58. P. Mahala, A. Kumar, S. Nayak, S. Behura, C. Dhanavantri, O. Jani, *Superlattice Microst.*, **92**, 366 (2016).

59. K. T. Chern, N. P. Allen, T. A. Ciarkowski, O. A. Laboutin, R. E. Welser, and L. J. Guido, *Mater. Sci. Semicond. Process.*, **55**, 2 (2016).
60. S. Hassan, Humaira, and M. Asghar, *IEEE conf. ICCSN* (2010).
61. J. Millan, P. Godignon, X. Perpina, A.P. Tomas, and J. Rebollo, *IEEE Trans. Power Electron., **29**,* 5 (2013).
62. U. K. Mishra, P. Parikh, and Y.F. Wu, *Proc. IEEE*, **90**, 6 (2002).
63. H. Ishida, R. Kajitani, Y. Kinoshita, H. Umeda, S. Ujita, M. Ogava, K. Tanaka, T. Morita, S. Tamura, M. Ishida and T. Ueda, *IEEE conf. IEDM* (2016).
64. N. Ikeda, Y. Niiyama, H. Kambayashi, Y. Sato, T. Nomura, S. Kato, and S. Yoshida, *Proc. IEEE*, **97**, 7 (2010).
65. Y. Wu, M. J. Mitos, M. L. Moore, and S. Heikman, *IEEE Electron Device Lett.*, **29**, 8 (2008).
66. W. Saito, T. Nitta, Y Kakiuchi, Y. Saito, K. Tsuda, I. Omura, and M. Yamaguchi, *IEEE Electron Device Lett.*, **29**, 1 (2008).
67. X. Huang, Z. Liu. Q. Li, and F. C. Lee, *IEEE Trans. Power Electron.*, **29**, 5 (2014).
68. D. Reusch, and J. Strydom, *IEEE conf. APEC* (2014).
69. M. Lu, G. G. Zhang, K. Fu, G. H. Yu, D. Su, and J. F. Hu, *Energ. Convers. Manage.*, **52**, 4 (2011).
70. E. B. Treidel, O. Hilt, R. Zhytnytska, A. Wentzel, C. Meliani, J. Wurfl, and G. Trankle, *IEEE Electron Device Lett.*, **33**, 3 (2012).
71. Y. Huang, X. Duan, Y. Cui, and C. M. Lieber, *Nano Letters*, **2**, 2 (2002).
72. J. Gassmann, P. Watson, L. Kehias, and G. Henry, *IEEE conf. MTT-S* (2007).
73. T. Dietl, H. Ohno, F. Matsukura, J. Cibert, and D. Ferrand, *Science*, **287**(5455), 1019 (2000).
74. M. Schilfgaarde and O. Mryasov, *Physical Review B*, **63**(23), 233205, (2001).
75. G. Das, B. Rao, P. Jena and Y. Kawazoe, *Computational materials science*, **36**(1), 84 (2006).
76. B. Rao and P. Jena, *Phys. Rev. Lett.*, **89**(18), 185504 (2002).
77. M. Kane, M. Strassburg, A. Asghar, W. Fenwick, J. Senawiratne, Q. Song, C. Summers, Z. Zhang, N. Dietz, and I. T. Ferguson, *Materials Science and Engineering B*, **126**(2), 230 (2006).
78. V. Dierolf, I. Ferguson and J Zavada, *Rare Earth and Transition Metal Doping of Semiconductor Materials: Synthesis, Magnetic Properties and Room Temperature Spintronics*, p. 342 (2016).
79. J. Kim, A. Ionescu, R. Mansell, I. Farrer, F. Oehler, C. Kinane, J. Cooper, N. Steinke, S. Langridge, R. Stankiewicz and C. Humphreys, R. Cowburn, S. Homles and C. Barnes, *J. Appl. Phys.*, **121**(4), 043904 (2017).
80. Z. Zhou, H. Wang, Z. Yang, Z. Ai, L. Guo and C. Liu, *J. Alloys and Compounds*, **658**, 800 (2016).
81. S. Gupta, Z. Tahir, A. Melton, E. Malguth, H. Yu, Z. Liu, X. Liu, J. Schwartz, and I. Ferguson, *Journal of Applied Physics*, **110**(8), 083920 (2011).
82. S. Dhar, L. Pérez, O. Brandt, A. Trampert, K. Ploog, J. Keller and B. Beschoten, *Physical Review B*, **72**(24), 245203 (2005).
83. K. Hoang, *physica status solidi (RRL)-Rapid Research Letters*, **10**(12), 915 (2016).

84. F. Lo, C. Huang, K. Chou, J. Guo, H. Liu, V. Ney, A. Ney, S. Shvarkov, S. Pezzagna, D. Reuter, C. Chia, M. Chern, A. Wieck and J. Massies, *Journal of Applied Physics*, **116**(4), 043909 (2014).

85. H. Sekiguchi, S. Nishikawa, T. Imanishi, K. Ozaki, K. Yamane, H. Okada, K. Kishino and A. Wakahara, *Jap. J. Appl. Phys*, **55**(5S), 05FG07 (2016).

86. V. Dierolf, I. Ferguson and J. Zavada, *Rare Earth and Transition Metal Doping of Semiconductor Materials: Synthesis, Magnetic Properties and Room Temperature Spintronics*, p. 298 (2016).

87. V. Dierolf, I. Ferguson and J. Zavada, *Rare Earth and Transition Metal Doping of Semiconductor Materials: Synthesis, Magnetic Properties and Room Temperature Spintronics*, p. 268 (2016).

88. S. Dhar, O. Brandt, M. Ramsteiner, V. Sapega and K. Ploog, *Phys. Rev. Lett.*, **94**(3), 037205 (2005).

89. Y. Kong, L. Liu, S. Xia, Y. Diao, H. Wang and M. Wang, *Optical and quantum electronics*, **48**(11), 493 (2016).

90. N. Kaleemullah, S. Ramsubramanian, R. Mohankumar, S. Munawar Basha, M. Rajagopalan and J. Kumar, *Solid State Communications*, **249**, 7 (2017).

91. X. Gao, B. Man, C. Zhang, J. Leng, Y. Xu, Q. Wang, M. Zhang and Y. Meng, *Journal of Alloys and Compounds*, **699**, 596 (2016).

92. B. Roul, M. Rajpalke, T. Bhat, M. Kumar, A. Kalghatgi, S. Krupanidhi, N. Kumar and A. Sundaresan. *Appl. Phys. Lett.*, **99**(16), 162512 (2011).

93. N. Lu, I. T. Ferguson, *Semicond. Sci. Technol.*, **28**(7), 074023 (2013).

94. I. Johnson, W. T. Choate, and A. Davidson, *Technology and Opportunities in U.S. Industry*, BCS Inc., Laurel, MD (2008).

95. E. N. Hurwitz, M. Asghar, A. Melton, B. Kucukgok, L. Su, M. Orocz, M. Jamil, N. Lu, I. T. Ferguson, *J. Electron. Mater.*, **40**(5), 513 (2011).

96. B. Kucukgok, B. Wang, A.G. Melton, N. Lu, I. T. Ferguson, *Phys. Status Solidi (c)*, **11**(3-4), 894 (2014).

97. C. W. Wu, Y. R. Wu, *J. Appl. Phys.*, **116**(10), 103707 (2014).

98. A. Sztein, H. Ohta, J. Sonoda, A. Ramu, J. E. Bowers, S. P. DenBaars, and S. Nakamura, *Appl. Phys. Express*, **2**(11), 111003 (2009).

99. S. Yamaguchi, R. Izaki, N. Kaiwa, and A. Yamamoto, *Appl. Phys. Lett.*, **86**(25), 252102 (2005).

100. N. Kaiwa, M. Hoshino, T. Yaginuma, R. Izaki, S. Yamaguchi, and A. Yamamoto, *Thin Solid Films*, **515**(10), 4501 (2007).

101. A. AlShaikhi and G. P. Srivastava, *Phys. Rev. B*, **76**(19), 195205 (2007).

102. H. H. Huang, I. L. Lu, and Y. R. Wu, *Phys. Status Solidi (a)*, **208**(7), 1562 (2011).

103. S. Yamaguchi, R. Izaki, N. Kaiwa, S. Sugimura, and A. Yamamoto, *Appl. Phys. Lett.*, **84**(24), 5344 (2004).

104. A. Sztein, H. Ohta, J. E. Bowers, S. P. DenBaars, and S. Nakamura, *J. Appl. Phys.*, **110**(12), 123709 (2011).

105. B. Kucukgok, X.Wu, X. Wang, Z. Liu, I. T. Ferguson, and N. Lu, *AIP Advances*, **6**(2), 025305 (2016).

106. W. Liu and A. A. Balandin, *J. Appl. Phys.*, **97**(7), 073710 (2005).

107. A. Sztein, *J. Appl. Phys.*, **113**(18), 183707 (2013).

108. A. Sztein, *Appl. Phys. Lett*., **104**(4), 042106 (2014).

109. B. N. Pantha, R. Dahal, J. Li, J. Y. Lin, H. X. Jiang, G. Pomrenke, *J. Elec. Mat*., **38**, 1132 (2009).

110. A. Sztein1, J. E. Bowers, S. P. DenBaars, and S. Nakamura, *J. Appl. Phys*., **112**, 083716 (2012).

111. E. A. Burgett, E. N. Hurwitz, N. E. Hertel, C. J. Summers, J. Nause, N. Lu, I. T. Ferguson, Handbook of Zinc Oxide and Related Materials, Chapter 12. Growth of ZnO for Neutron Detectors, p.435 (2012).

112. A. Owens, A. Peacock, *Nucl. Instr. Meth. Phys. Res*., **531**(1), 18 (2004)

113. H. P. D. Schenk, S. I. Borenstain, A. Berezin, A. Schön, E. Cheifetz, A. Dadgar, and A. Krost, *J. Crys. Growth*, **311**(16), 3984 (2009).

114. Y. Huang, A. Melton, B. Jampana, M. Jamil, J. H. Ryou, and R. D. Dupuis, *J. Appl. Phys*., **110** (6), 064908 (2011).

115. G. Wang, K. Fu, C. S.Yao, D. Su, G. G. Zhang, J. Y. Wang, M. Lu, *Nucl. Instr. Meth. Phys. Res*., **663**(1), 10 (2012).

116. S. Gautier, G. Orsal, T. Moudakir, N. Maloufi, F. Jomard, M. Alnot, Z. Djebbour, A. A. Sirenko, M. Abid, K. Pantzas, I. T. Ferguson, P. L. Voss, and A. Ougazzaden, *J. Cryst. Growth*, **312** (5), 641 (2010).

117. S. Gupta, T. Zaidi, A. Melton, E. Malguth, H. Yu, Z. Liu, X. Liu, J. Schwartz, I. T. Ferguson, *J. Appl. Phys*., **110**(8), 083920 (2011).

118. A. G. Melton, E. Burgett, N. Hertel, I. T. Ferguson, *MRS Proc*., 1396, mrsf11-1396-o04-08 (2012)

119. A. G. Melton, E. Burgett, T. Xu, N. Hertel, and I. T. Ferguson, *Phys. Status Solidi (c)*, **9** (3□4), 957 (2012).

120. A. Y. Polyakov, N. B. Smirnov, A. V. Govorkov, A. V. Markov, E. A. Kozhukhova, I. M. Gazizov, N. G. Kolin, D. I. Merkurisov, V. M. Boiko, A. V. Korulin, V. M. Zalyetin, S. J. Pearton, I.H. Lee, A. M. Dabiran, and P. P. Chow, *J. Appl. Phys*., **106**(10), 103708 (2009).

121. P. Mulligan, J. Wang, L. Cao, *Nucl. Instr. Meth. Phys. Res*., **719**, 13 (2013).

122. J. Kamimura, P. Bogdanoff, J. Lähnemann, C. Hauswald, L. Geelhaar, S. Fiechter, and H. Riechert, *J. Am. Chem. Soc*., **135**, 10242 (2013).

123. M. G. Kibria, H. P. T. Nguyen, K. Cui, S. Zhao, D. Liu, H. Guo, M. L. Trudeau, S. Paradis, A. Hakima, and Z. Mi, *ACS nano*, 7, 7886 (2013).

124. N. Iqbal, I. Khan, Z. H. Yamani, and A. Qurashi, *Scientific Reports*, **6**, 32319 (2016).

125. H. Pan, *Renewable and Sustainable Energy Reviews*, **57**, 584 (2016).

126. S. Leung, Q. Zhang, F. Xiu, D. Yu, J. C. Ho, D. Li, and Z. Fan, *J. Phys. Chem. Lett*., **5**, 1479 (2014).

127. I. M. Pryce, D. D. Koleske, A. J. Fischer, and H. A. Atwater, *Appl. Phys. Lett*., **96**, 153501 (2010).

128. G. Sun, J. B. Khurgin, and R. A. Soref, *J. Opt. Soc. Am. B*, **25**(10), 1748 (2008).

129. T. N. Oder, J. Shakya, J. Y. Lin, and H. X. Jiang, *Appl. Phys. Lett*., **83**, 1231 (2003).